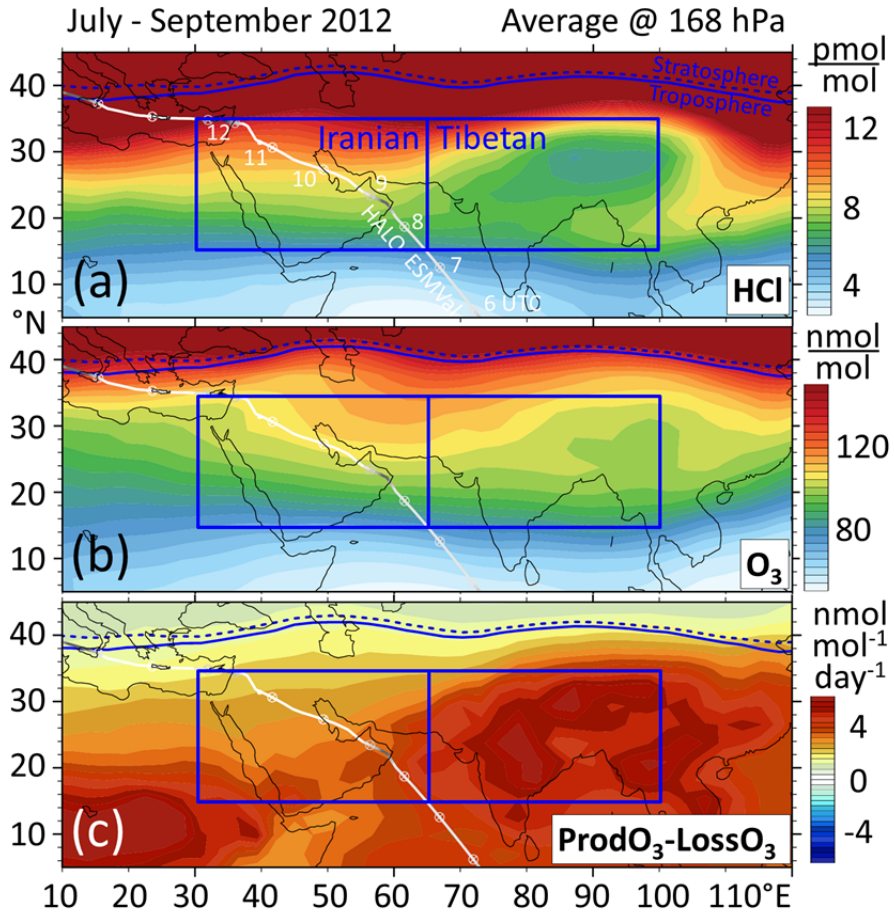

Figure S1. Trace gas mixing ratios and net O_3 production as simulated by EMAC at 168 hPa for the monsoon months of 2012. The Iranian and Tibetan domains correspond to the regions used for lateral averaging throughout the paper (e.g. Figs. 2 - 5, S4 – S10). The Iranian region was traversed by the HALO ESMVal campaign during a flight from Male (Maledives) to Larnaca (Cyprus) on 18 September 2012. HALO was flying in the upper troposphere where the flight track is colored white and dived to the lower troposphere where it is grey. Beads show the HALO positions at full UTC hours.

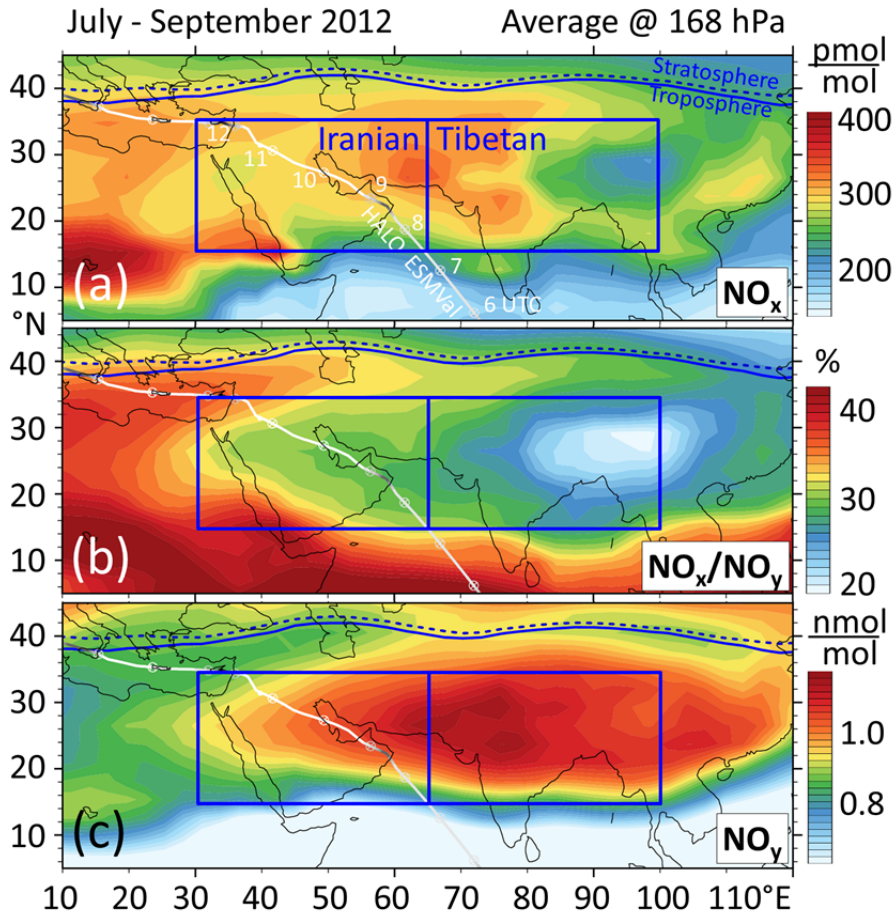

Figure S2. As Fig. S1, but for different tracers.

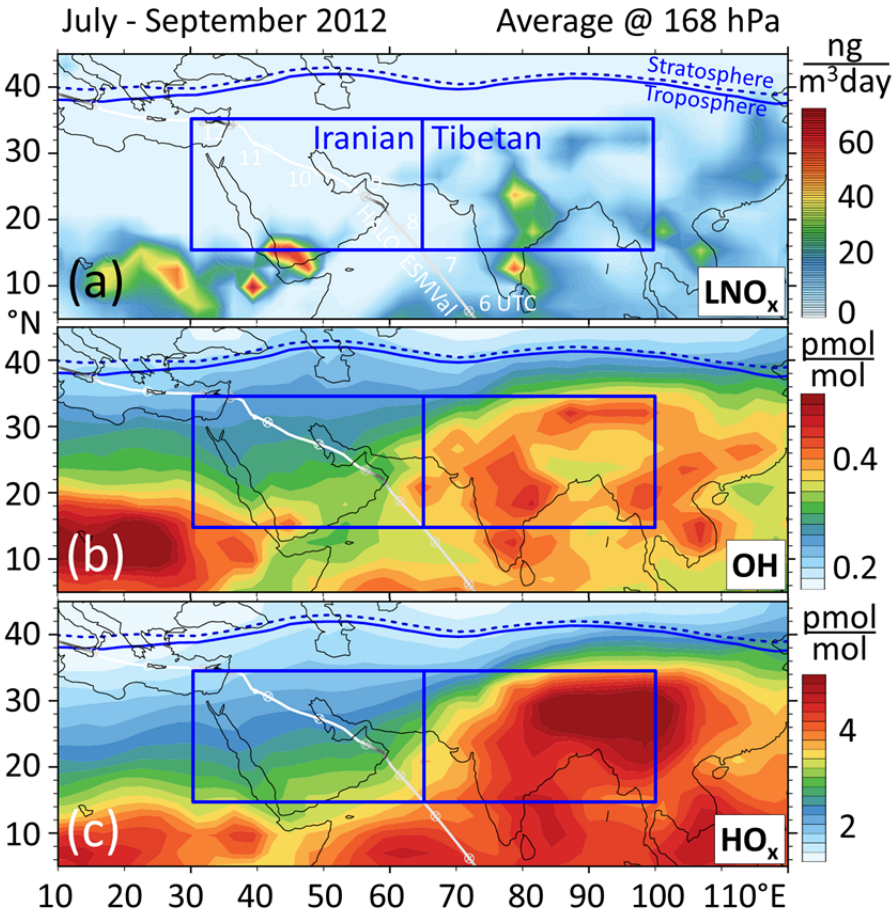

Figure S3. As Fig. S1, but for different tracers.

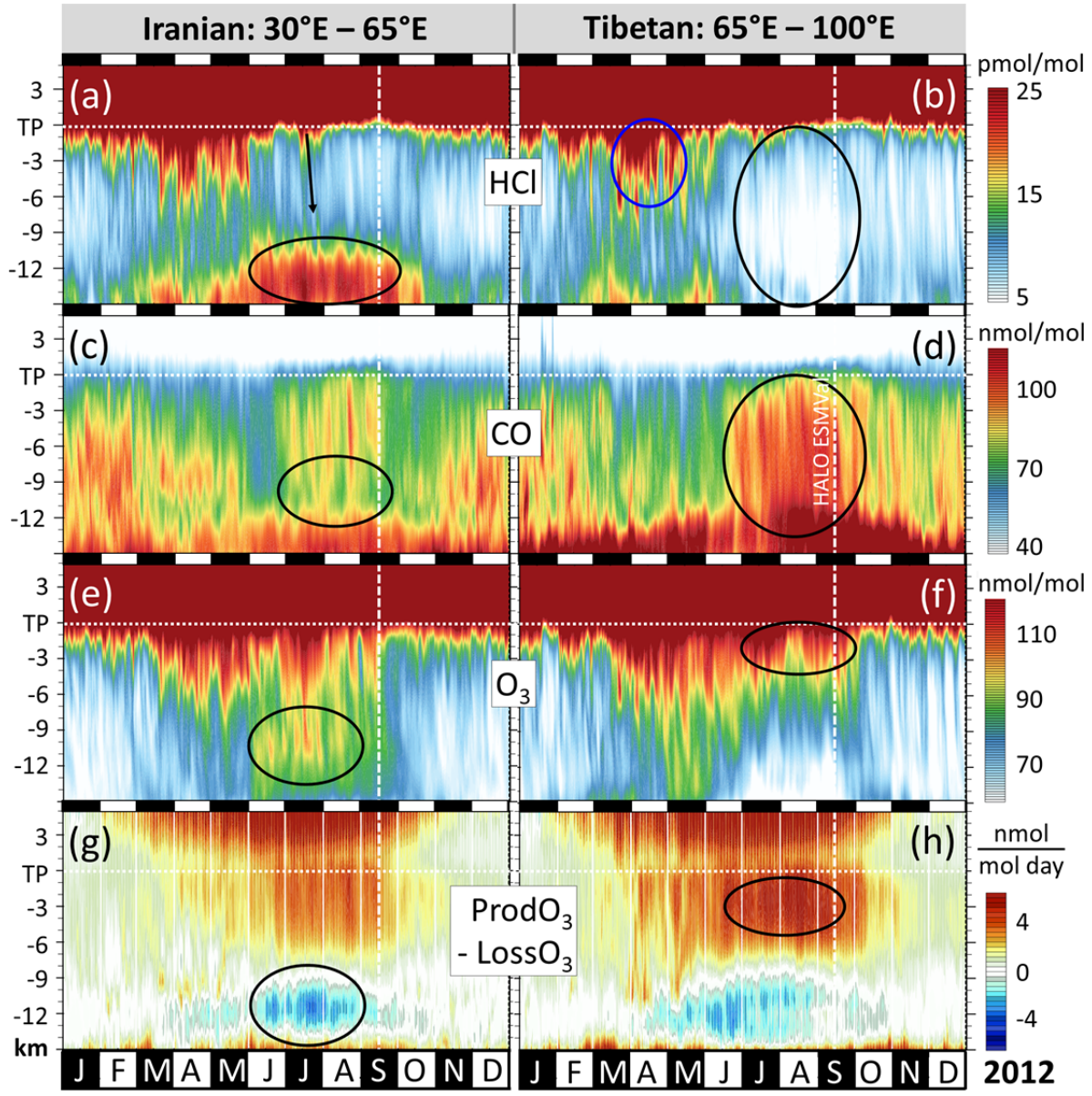

Figure S4. Evolution of simulated trace gas profiles and related diagnostics throughout 2012 in the ASMA region. Figure S4 is identical to Fig. 2, except that vertical coordinates are given as distance to the tropopause ("TP") here. Compared to the pressure-based vertical axis' used in Fig. 2, the tropopause region is resolved better here – at the expense of the middle troposphere. All values are grid-cell dry air mass weighted averages from 15°N to 35°N, respectively for the western (30° - 65°E) and eastern (65° - 100°E) parts of the ASMA (see Figs. 1, S1, S2, S3). The features marked by circles and arrows are the same as in Fig. 2 and discussed in the text.

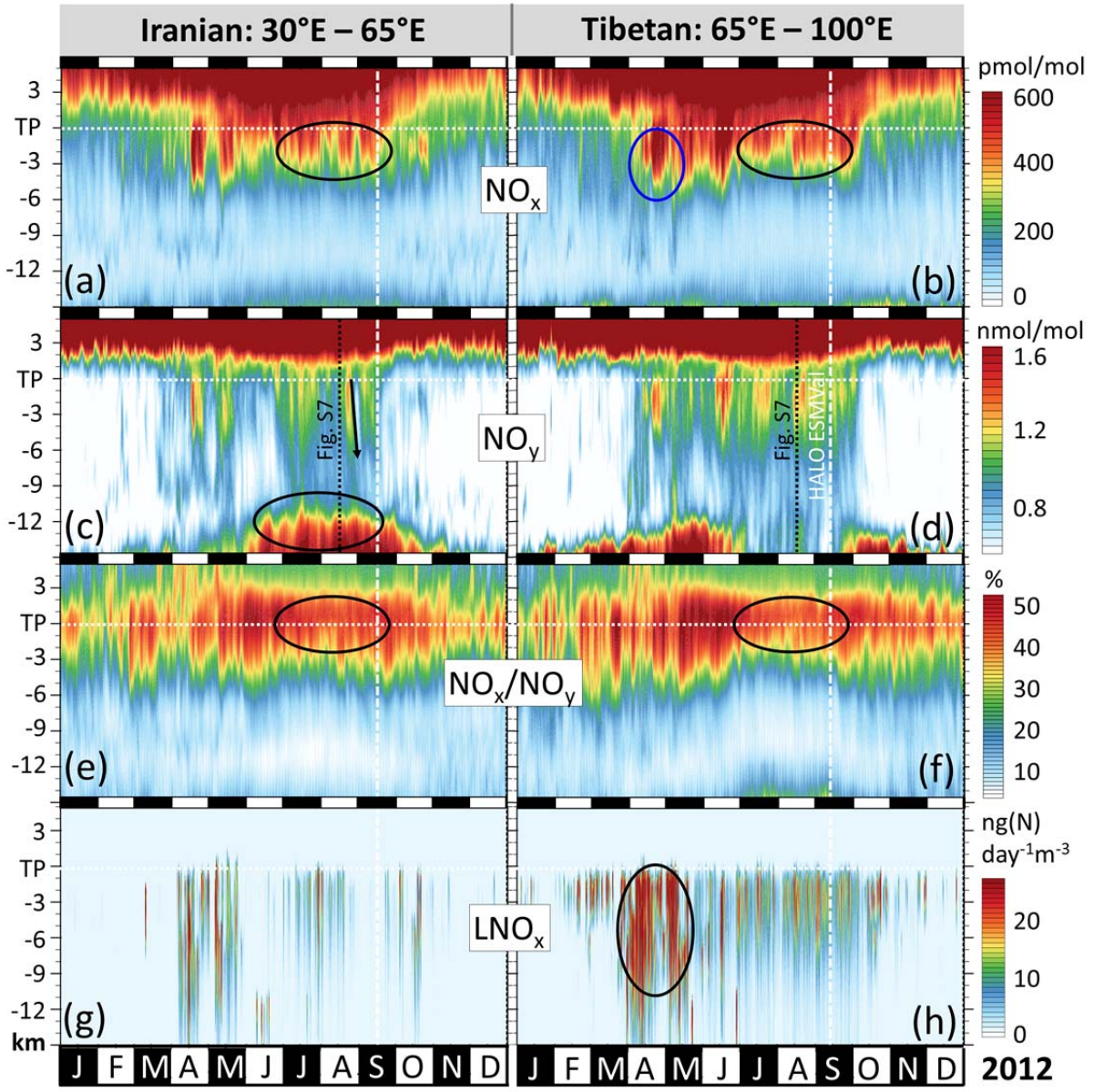

Figure S5. As Fig. S4, but for different tracers. The individual NO_y-profiles shown in Fig. S7 are indicated in panels c and d.

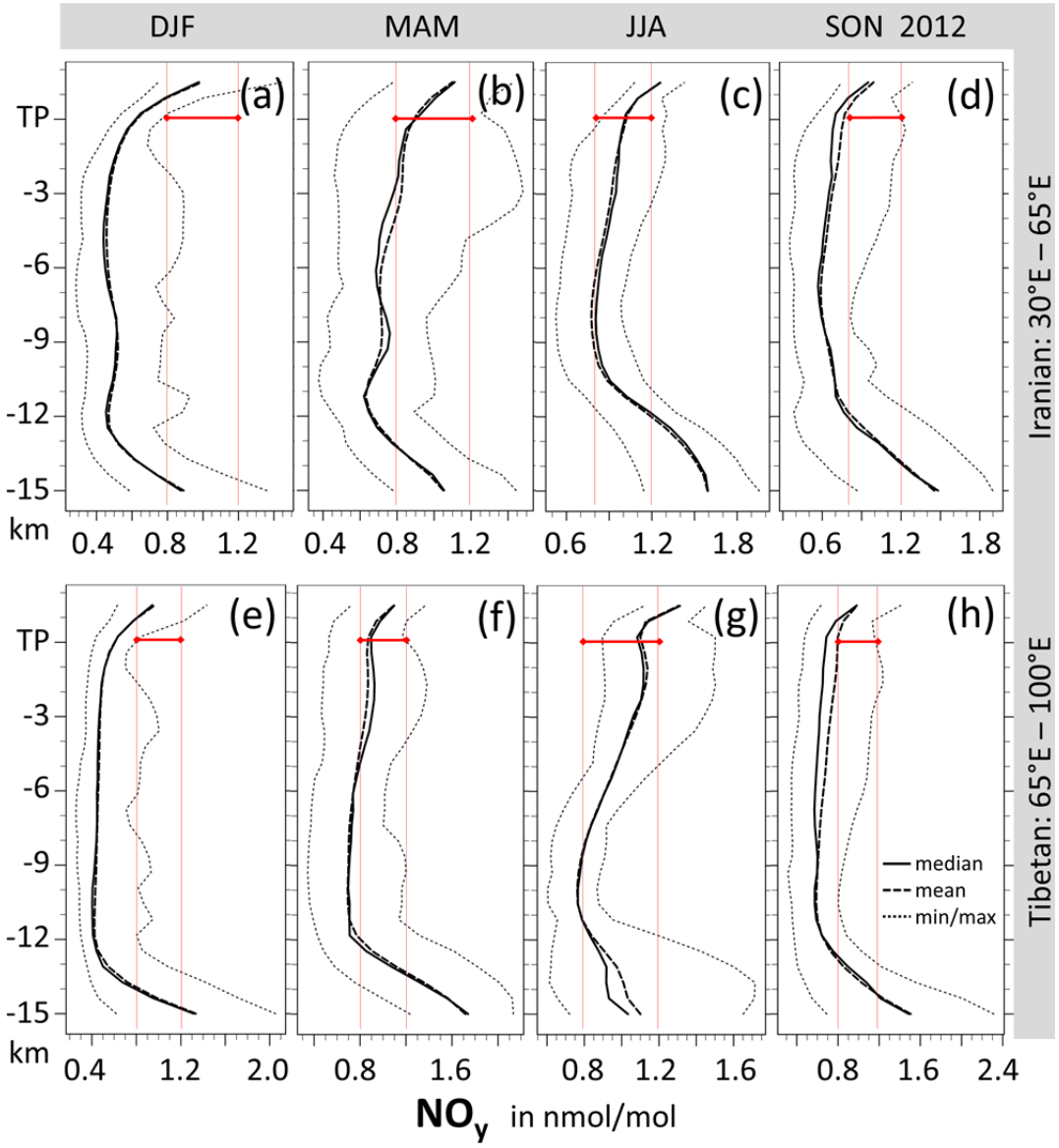

Figure S6. EMAC-simulated three-monthly mean NOy-profiles in the Iranian and Tibetan regions, respectively. Note that the panels cover different ranges of NOy mixing ratios. Auxiliary red lines always mark the interval 0.8 to 1.2 nmol/mol, as well as the tropopause in that interval.

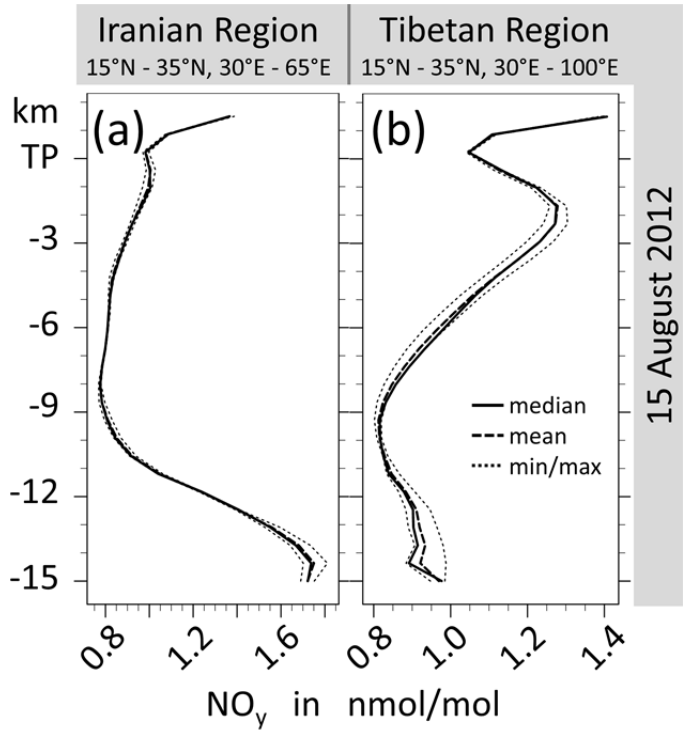

Figure S7. Simulated profiles of NOy as simulated for 15 August 2012. These are examples of a C-shaped profile in the Iranian region (a) and an E-shaped profile in the Tibetan region (b).

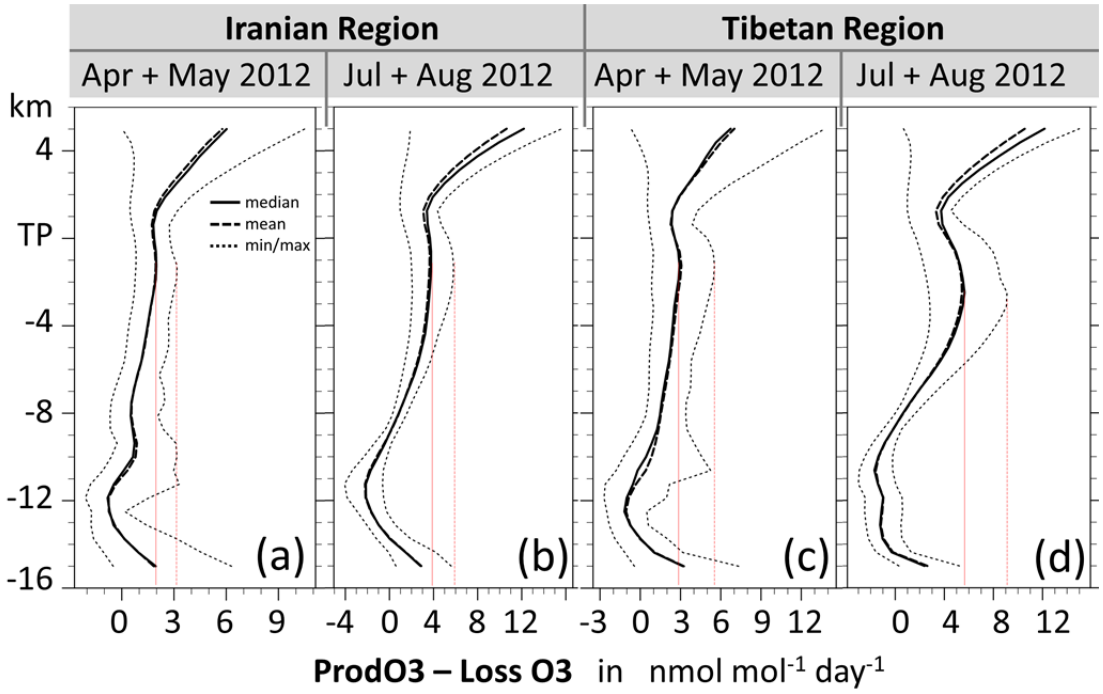

Figure S8. Simulated profiles of net O_3 production in the Tibetan region. Auxiliary red lines indicate the mean and maximum net O_3 production in the UT, which are both higher in summer than in spring. See also Fig. S4h for the evolution of these profiles throughout 2012.

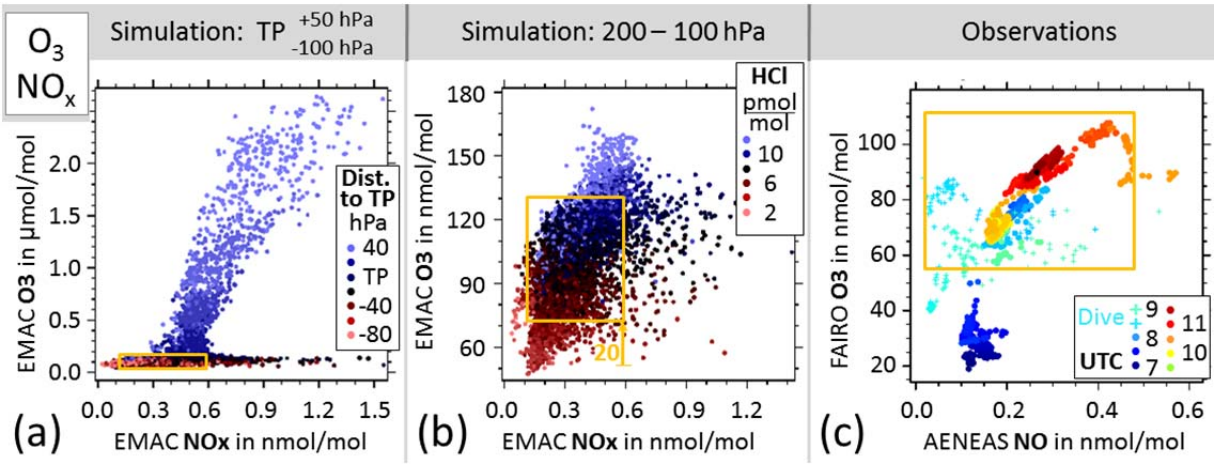

Figure S9. As Fig. 4, but for NO_x vs O_3. Panel (c) shows NO instead of NO_x, because only NO was measured. At daytime, i.e. at the time of the measurements, NO is good proxy for NO_x. Simulated O_3 and NO_x increase in the stratosphere with a higher O_3/NO_x ratio than in the troposphere (Fig. S9a). At NO_x mixing ratios of more than 0.7 nmol/mol the corresponding O_3 mixing ratios would allow distinguishing stratospheric influence from tropospheric in situ production, but the range covered by the HALO ESMVal measurements is just at the intersection of stratospheric and tropospheric branch (orange box in Fig. S9a). Similar HCl mixing ratios are simulated throughout the ranges of measured NO_x and O_3 (orange box in Fig. S9b). Measurements of increased NO_x in combination with increased O_3 (upper right corner of the orange boxes in Fig. S9) are compatible with both, increased in situ O_3 production and influence from the stratospheric branch. Consequently almost all measurements in the ASMA filament are well correlated on the scale of all our ASMA measurements (Fig. S9c). As discussed in the accompanying paper, the positive correlation between NO and O_3 is attributed to enhanced O_3 production due to increased NO, if NO also positively correlates with NO_y.

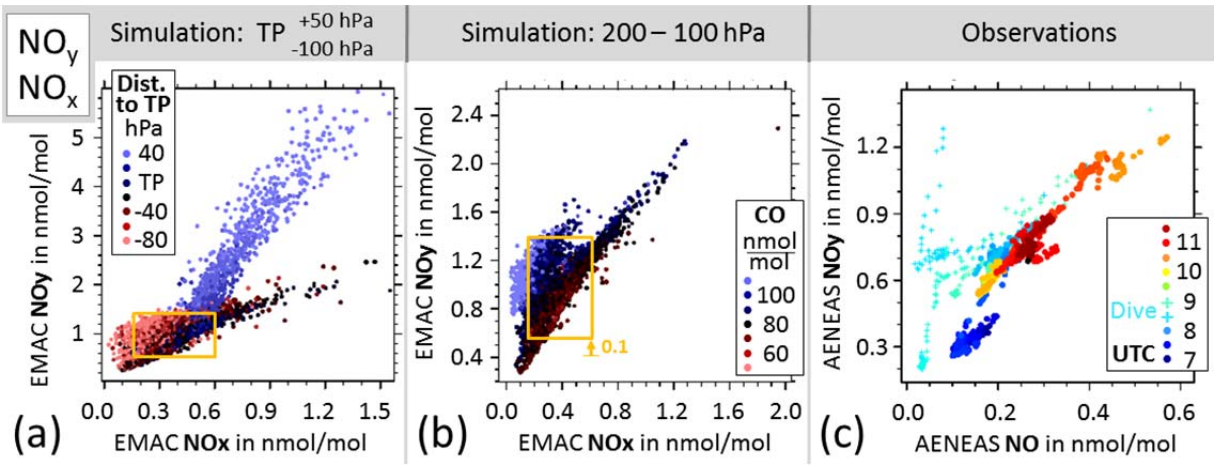

Figure S10. As Fig. S9, but for NO_x vs NO_y. There are three distinct regions in Fig. S10a: a blueish stratospheric branch, a dark TL branch, and a reddish UT region. As a consequence of the local NO_y minimum directly above the tropopause (Figs. 3d, S5, S7), the most decreased NO_y mixing ratios in Fig. S10a also show up in samples taken from near the tropopause. Measured NO and NO_y values in the ASMA filament are well correlated (Fig. S10c), consistent with almost constant NOx/NOy ratios in the UT (Figs 3ef). Furthermore, the simulation shows much more scatter in NO_x-vs-O_3 space than the observations. The narrow, linear distribution of the ASMA measurements in Figs. S9c and S10c indicates that all parts of the transected filament had similar sources of reactive nitrogen. This is consistent with Appendix A, where lightning is found to be the dominating source of reactive nitrogen in the ASMA. In the accompanying study is also shown that the filament had seen convection at the eastern ASMA flank three to five days before the measurements. Thus the gradients of NO and NO_y in Fig. S9c and Fig. S10c can be explained by different amounts of lightning NO_x of approximately the same age.

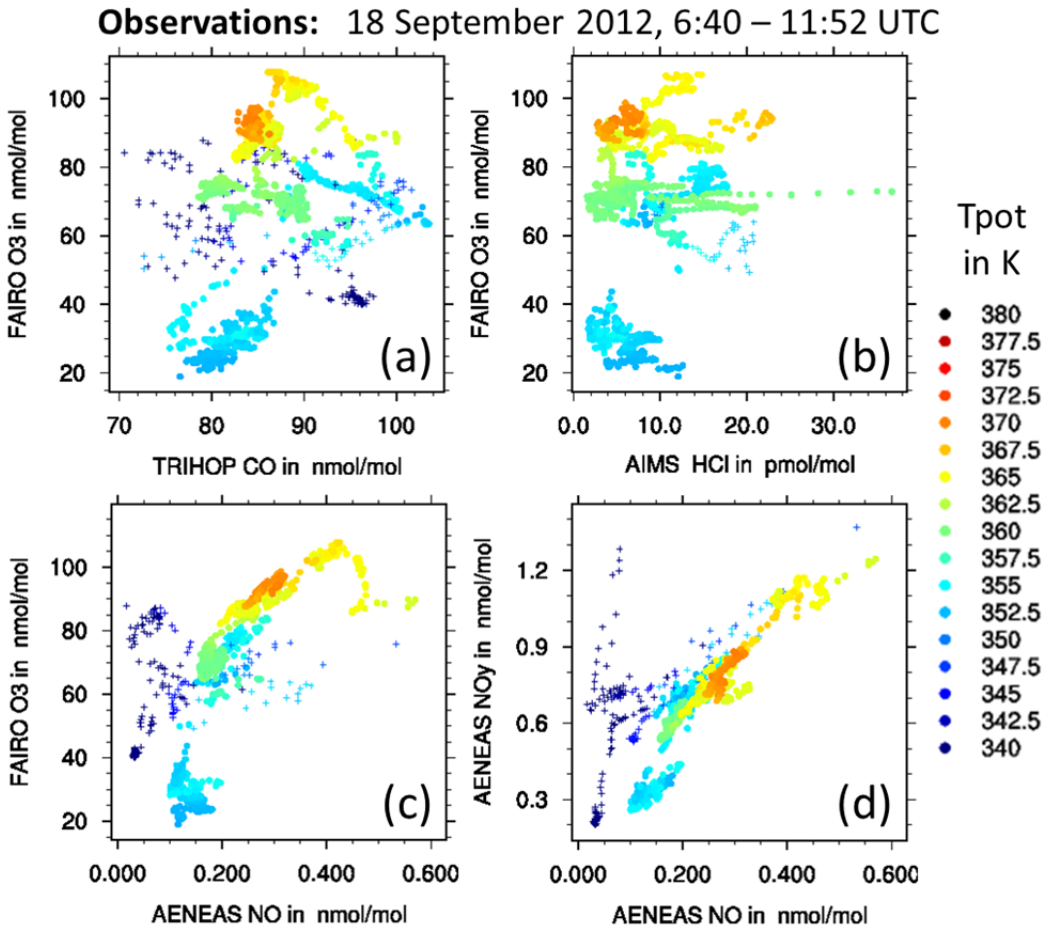

Figure S11. Panels a, b, c, d show measured data from the HALO ESMVal flight from Male to Larnaca as Figs. 4c, 5c, S9c, S10c, respectively. The only difference is that the samples here are color coded by their potential temperatures. During the dive (POI4: crosses) potential temperatures were lower than shown, but the color scale is cut off at 340 K. See also Fig. 7 and Fig. S12 for simulated potential temperatures in the ASMA region.

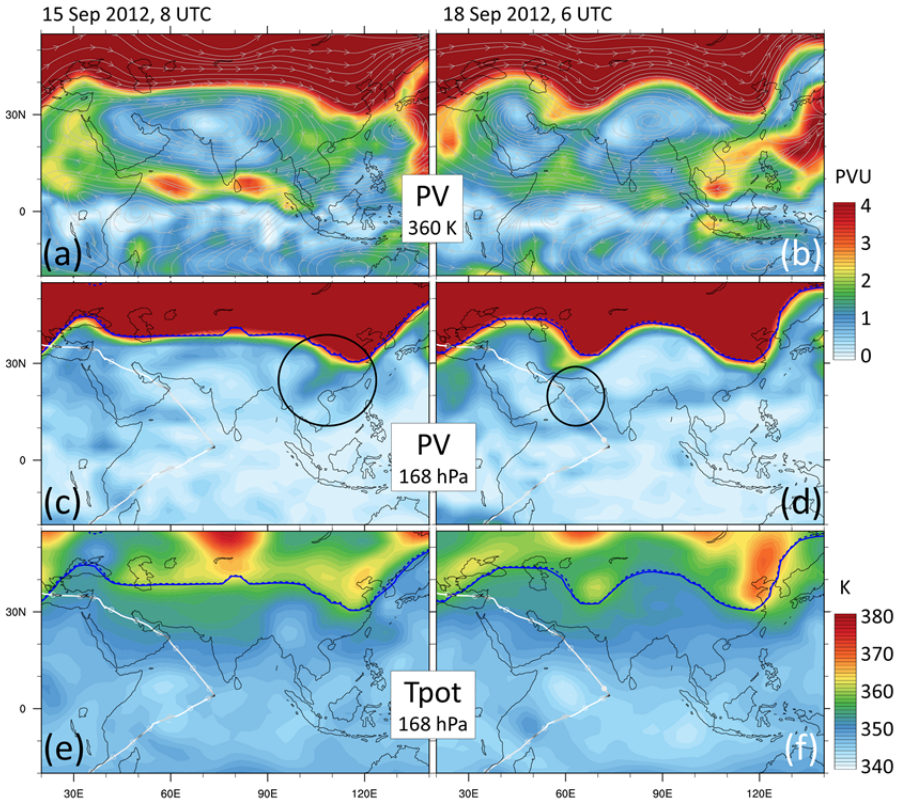

Figure S12. EMAC simulated potential vorticity at the 360 K isentropic level (panels a, b) and the 168 hPa pressure level (panels c, d). The black circle in panel c shows the entrainment of TL air, which occurred when the air mass corresponding to POI3 was passing the eastern ASMA flank. Panels b, d, f show simulated snapshots 2 hours before POI3, with the region of POI3 marked in panel d. The corresponding potential temperatures are shown in panels e and f. Note that TL layer entrainments are visible in PV, but are hardly detected by Tpot.

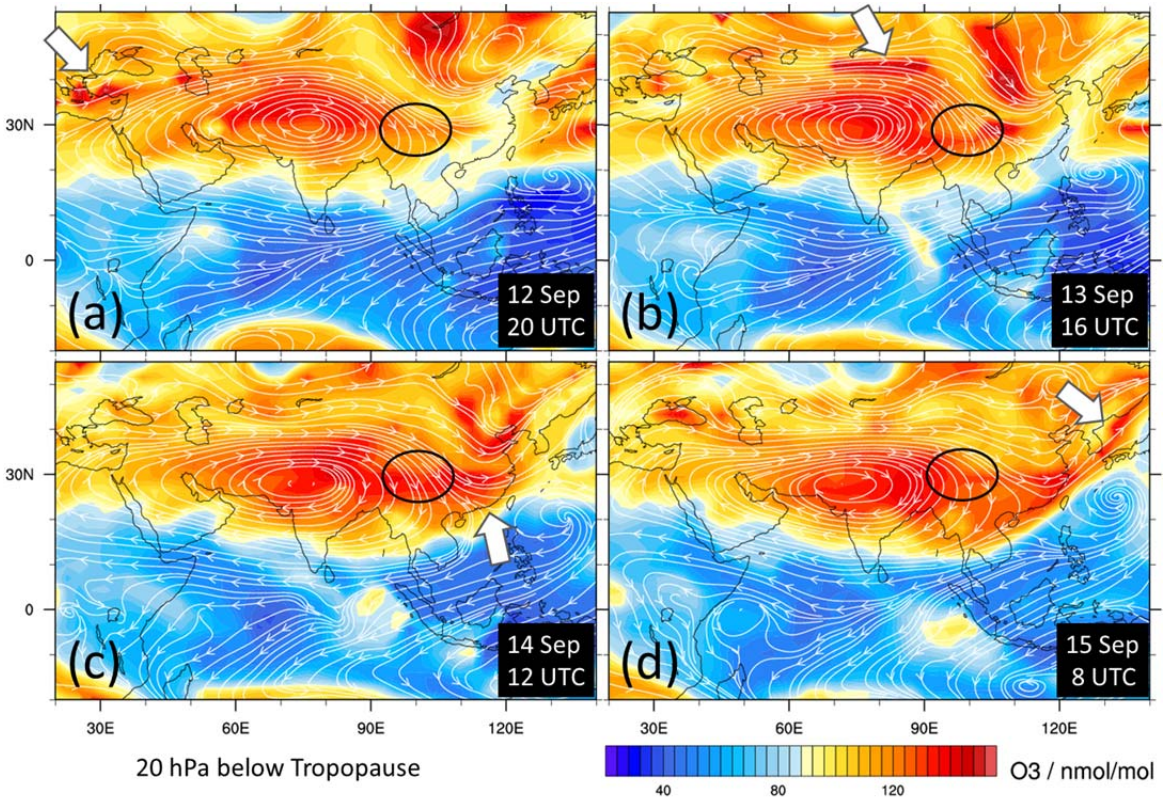

Figure S13. Sequence of O_3 mixing ratios in the ASMA region and streamlines as simulated by EMAC for a layer 20 hPa below the tropopause. This layer was chosen to illustrate O_3 variations and transport just below the TP. EMAC tropopause height varies spatially and temporally, as it is diagnosed each time step, according to the WMO definition between 30°S and 30°N, and by PV = 3.5 PVU otherwise. Note that the layer may not, or may only partially show altitudes that contributed to the HALO measurements. The streamlines are based on instantaneous wind fields and thus not identical to backward trajectories. Grey arrows indicate a pocket of increased O_3, which originated in the tropopause folding region over the Eastern Mediterranean. It is picked up by the ASMA circulation and transported along the northern ASMA flank. The pocket passes the eastern ASMA flank before the time (last panel), when the air mass to be encountered by HALO arrived there (region indicated by black circles). However, a part of the increased O_3 patch might have been entrained in the divergent flow there, diverted away from the TP and carried along the southern ASMA flank back east.

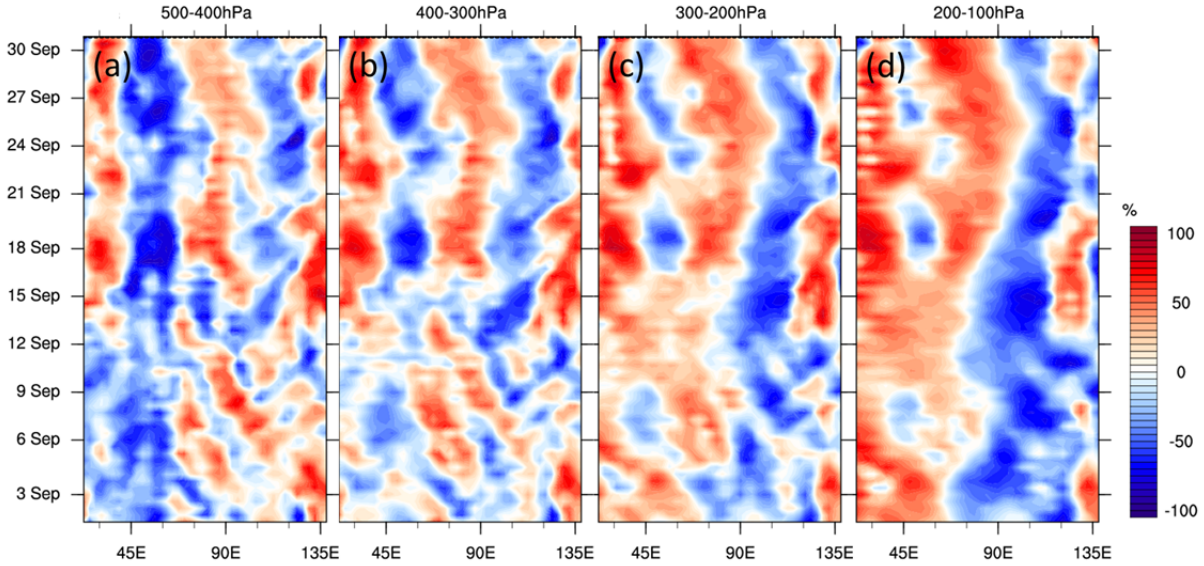

Figure S14. Evolution of meridional wind fraction, as averaged over 10°N – 40°N and the respective altitude range. The results are based on 10-hourly output of EMAC simulation RC1SD-base-10a for September 2012 in the ASMA region. Weighting considers the dry air mass in the cell, and completely or partly stratospheric cells are ignored. At a given time, each red-blue-pair (from left to right) represents an anticyclone, because positive values indicate overall northward meridional wind fractions. Blue shades represent mainly southward wind fractions.

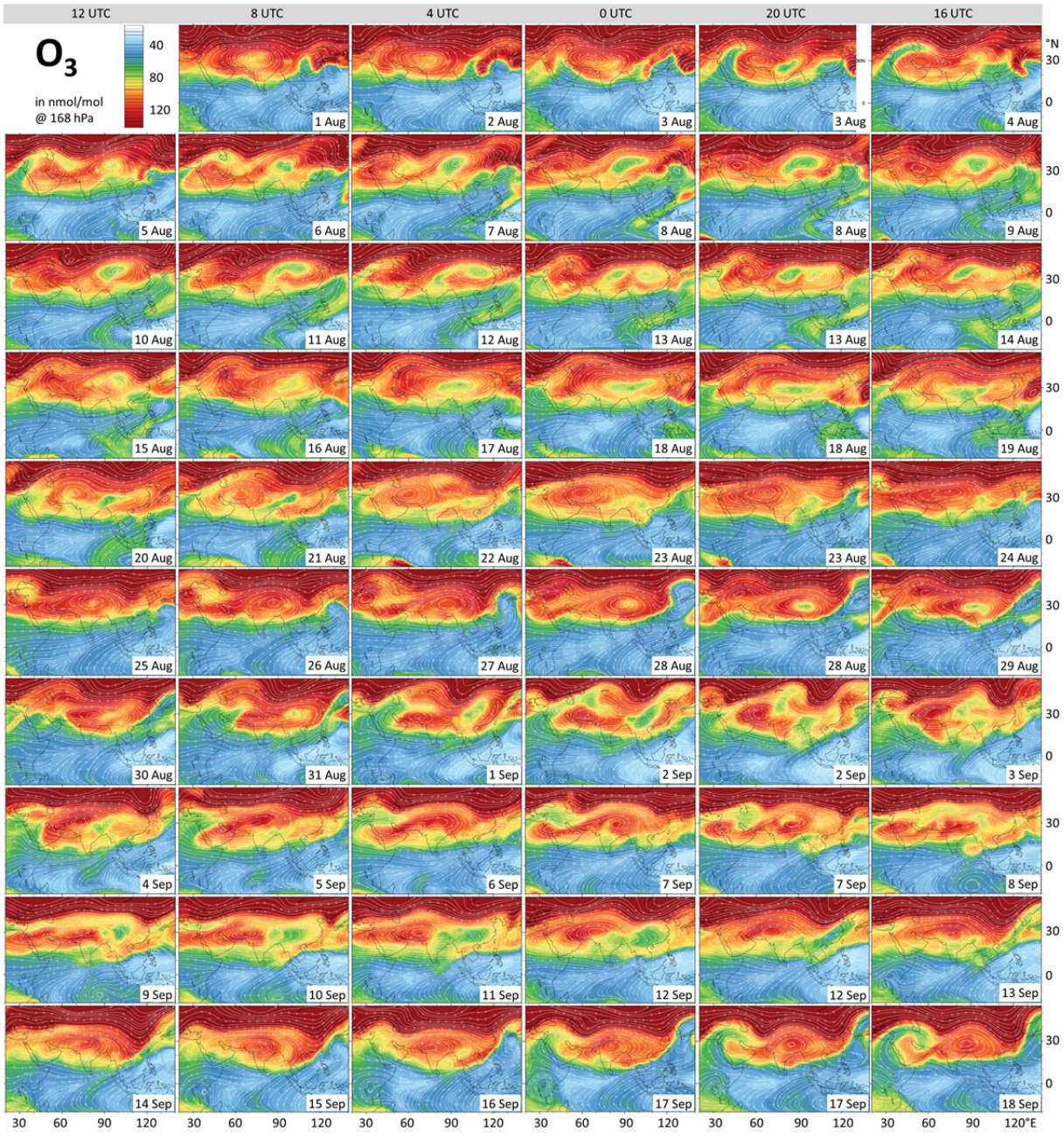

Figure S15. EMAC simulated O_3 mixing ratios and streamlines at 168 hPa in the ASMA region. The snapshots are 20 hours apart and cover the period from 1 August to 18 September 2012.

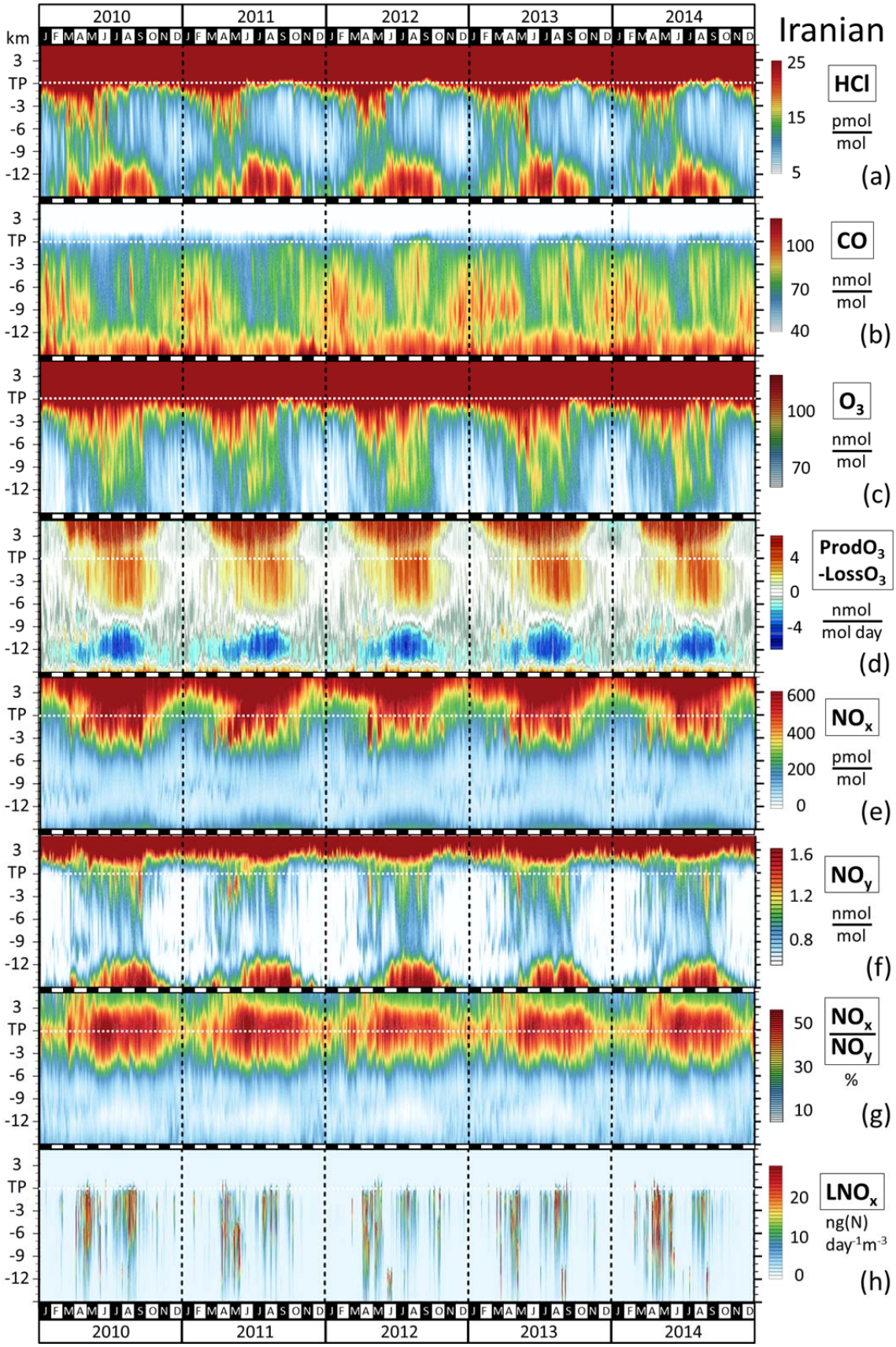

Figure S16. Evolution of simulated trace gas profiles and related diagnostics for the years 2010 - 2014 in the Iranian ASMA region. The column for the year 2012 is identical to the corresponding panels in Figs. S4, S5.

References

Deckert, R., Jöckel, P., Grewe, V., Gottschaldt, K., and Hoor, P.: A quasi chemistry-transport model mode for EMAC, Geoscientific Model Development, 4, 195-206, 10.5194/gmd-4-195-2011, 2011.

Jöckel, P., Tost, H., Pozzer, A., Kunze, M., Kirner, O., Brenninkmeijer, C. A. M., Brinkop, S., Cai, D. S., Dyroff, C., Eckstein, J., Frank, F., Garny, H., Gottschaldt, K., Graf, P., Grewe, V., Kerkweg, A., Kern, B., Matthes, S., Mertens, M., Meul, S., Neumaier, M., Nützel, M., Oberländer-Hayn, S., Ruhnke, R., Runde, T., Sander, R., Scharffe, D., and Zahn, A.: Earth System Chemistry Integrated Modelling (ESCiMo) with the Modular Earth Submodel System (MESSy, version 2.51), Geosci. Model Dev. Discuss., 8, 8635–8750, 10.5194/gmdd-8-8635-2015, 2015.